

# Experimental studies of peptide bonds: Identification of the $C_7^{\text{eq}}$ conformation of the alanine dipeptide analog *N*-acetyl-alanine *N'*-methylamide from torsion-rotation interactions

R. J. Lavrich, D. F. Plusquellic, R. D. Suenram, G. T. Fraser, and A. R. Hight Walker  
*Optical Technology Division, National Institute of Standards and Technology,  
Gaithersburg, Maryland 20899-8441*

M. J. Tubergen  
*Department of Chemistry, Kent State University, Kent, Ohio 44242-0001*

(Received 15 August 2002; accepted 23 October 2002)

Rotational spectra of the biomimetic molecule, alanine dipeptide and the double  $^{15}\text{N}(^{15}\text{N}_2)$  isotopomer have been observed using a pulsed-molecular-beam Fourier transform microwave spectrometer. The spectra reveal tunneling splittings from the torsional mode structure of two of its three methyl rotors. The torsional states assigned include one *AA*-state and two *AE*-states (i.e., *AE* and *EA*) for each isotopomer. The *AA*-states are well-fit to *A*-reduction asymmetric-rotor Hamiltonians. The “infinite-barrier-limit” rotational constants of the  $^{14}\text{N}_2$  isotopomer are  $A = 1710.97(8)$  MHz,  $B = 991.89(9)$  MHz, and  $C = 716.12(6)$  MHz. The *AE*-states are analyzed independently using “high-barrier” torsion-rotation Hamiltonians, yielding observed-minus-calculated standard deviations of  $<400$  kHz. The fits improve substantially ( $>100$ -fold for the  $^{15}\text{N}_2$  isotopomer) when analyzed in a  $\rho$ -axis frame where  $\rho_b = \rho_c = 0$ . The best-fit torsion-rotation parameters provide accurate  $V_3$  barriers and  $C_3$  rotor axis angles for both methyl groups. The observed angles are shown to uniquely correlate with those calculated for the acetyl and amide methyl groups in the  $C_7^{\text{eq}}$  conformational form. The  $V_3$  barriers of the amide and acetyl methyl groups are  $84.0(3)$   $\text{cm}^{-1}$  and  $98.4(2)$   $\text{cm}^{-1}$  for the  $^{14}\text{N}_2$  and  $84.1(1)$   $\text{cm}^{-1}$  and  $98.65(8)$   $\text{cm}^{-1}$  for the  $^{15}\text{N}_2$  isotopomers, respectively. These results are in good agreement with prior geometry optimizations and with current  $V_3$  barrier calculations which predict the  $C_7^{\text{eq}}$  conformation as the lowest energy form in the gas phase. Under certain conditions, the spectrum is dominated by transitions from a thermal decomposition product formed by dehydration of alanine dipeptide. This molecule is tentatively identified as 3,5-dihydro-2,3,5-trimethyl-(9CI) 4H imidazole-4-one (CAS registry #32023-93-1). © 2003 American Institute of Physics. [DOI: 10.1063/1.1528898]

## I. INTRODUCTION

*N*-acetyl-alanine *N'*-methylamide (AAMA) and *N*-formyl-alanine amide (FAA) serve as models for protein conformation studies<sup>1–9</sup> because they possess two peptide bonds, and like polypeptides and proteins, the backbone conformation is determined by the orientation about the  $\text{N}-\text{C}^\alpha$  and  $\text{C}'-\text{C}^\alpha$  single bonds (these torsional angles are denoted  $\phi$  and  $\psi$ , respectively). *Ab initio* calculations consistently identify the  $C_7^{\text{eq}}$  conformation ( $\phi = -86^\circ$  and  $\psi = 79^\circ$ ) (Ref. 3) as the lowest energy backbone structure of the dipeptide analogs. This structure, shown in the top panel of Fig. 1, is characterized by a seven-membered ring stabilized by a strained, 2.22 Å intramolecular hydrogen bond from the amide nitrogen to the carbonyl oxygen; the alanine  $C_\beta$  is equatorial to the ring. *Ab initio* calculations also predict that the  $C_5$  conformation ( $\phi = -156^\circ$  and  $\psi = 161^\circ$ ) is between 1.7 and 7.4  $\text{kJ mol}^{-1}$  above the  $C_7^{\text{eq}}$  minimum, depending on the basis set and level of theory.<sup>7</sup> The lower panel of Fig. 1 shows that the  $C_5$  structure has a much more strained amide-to-carbonyl-oxygen hydrogen bond forming a five-membered ring. Other conformers of AAMA are estimated to be more than 10  $\text{kJ mol}^{-1}$  above the  $C_7^{\text{eq}}$  structure.

Gas-phase experiments, in which AAMA is isolated from nearest neighbor interactions, are necessary for understanding the intrinsic conformational preferences of AAMA and how these may be influenced by solvent environments. Results from isolated-molecule experiments can be directly compared to *ab initio* theoretical predictions. Some experimental evidence for the presence of both the  $C_7^{\text{eq}}$  and the  $C_5$  conformations of isolated AAMA comes from gas-phase electron-diffraction experiments.<sup>6</sup> These results, however, were tightly constrained to minimum-energy *ab initio* structures at relatively low levels of theory (HF/6-31G\*). Interestingly, recent calculations and liquid-crystal NMR experiments indicate that hydrogen bonding by four bridging water molecules may cause the polyproline II conformation ( $P_{\text{II}}$ ;  $\phi = -85^\circ$  and  $\psi = 160^\circ$ ) of AAMA to become predominant.<sup>10</sup>

Rotational spectroscopy is a proven technique for conformer identification and molecular structure determination. Different conformational isomers have unique, and often very different, moments of inertia and give rise to separate rotational spectra. Even structural isomers in conformationally challenging systems can be distinguished by rotational spectroscopy, as illustrated by investigations of 1-pentene

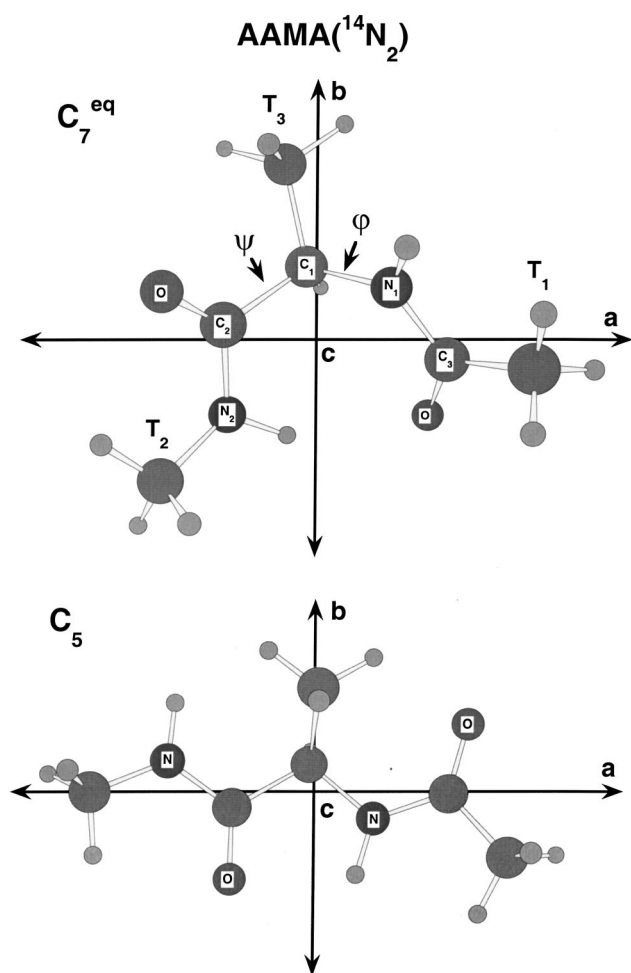


FIG. 1. *Ab initio* structures of the  $C_7^{eq}$  (top) and the  $C_5$  (bottom) conformations of AAMA. The Ramachandran angles,  $\phi$  and  $\psi$ , define the different conformations. Tunneling splitting are observed only for the  $T_1$  and  $T_2$  methyl groups.

through 1-dodecene.<sup>11–13</sup> Rotational spectra have been assigned to four of the five low-energy 1-pentene conformers<sup>11</sup> and seven of the thirteen 1-hexene conformers,<sup>12</sup> up to 15 unique conformer spectra have been assigned for 1-octene.<sup>13</sup> With sufficient isotopic data, rotational spectroscopy can also precisely determine structural features such as bond lengths, bond angles, and torsional angles. The torsional angles that define the different 1-pentene conformations, for example, were determined to within  $\pm 0.5^\circ$ .

The structures of an increasing number of amino acids, amino acid derivatives, and peptide mimetics have been investigated by rotational spectroscopy. Spectra have been reported for two conformations of the amino acids glycine<sup>14–18</sup> and alanine.<sup>19</sup> The conformers can be characterized by their intramolecular hydrogen bonds. The lowest-energy conformational isomer has an intramolecular hydrogen bond from the amine to the carbonyl oxygen while the second isomer has an acid-to-amino-nitrogen hydrogen bond. Extensive isotopic substitution has been employed, and the structures of both conformations of glycine are now accurately known. Rotational spectra of the amino acid derivatives alaninamide,<sup>20</sup> prolinamide,<sup>21</sup> valinamide,<sup>22</sup> and leucinamide<sup>23</sup> indicate that the energy ordering of their con-

formers differs from that of the amino acids. Spectra have been observed for only one conformation of alaninamide, valinamide, and prolinamide. These structures have intramolecular hydrogen bonds from the amide to the amine groups and are analogous to the higher energy amino acid conformation. Two conformations have recently been detected from leucinamide. Each retains the amide-to-amine hydrogen bonding scheme with differences occurring in the orientation of the isobutyl side chain. The amide-to-amine conformer is preserved in the alaninamide–water complex,<sup>24</sup> where the water interacts with the amide group, accepting a hydrogen bond from the amide and donating one to the carbonyl oxygen. A rotational spectrum and structure have also been reported recently for the cyclic dipeptide, diketopiperazine.<sup>25</sup> The backbone of the isolated molecule adopts a  $C_2$  symmetrical boat conformation, in contrast to the planar configuration observed in the crystal phase.<sup>26</sup>

The extensive theoretical interest in the AAMA model dipeptide and the limited experimental data characterizing the structure of the isolated molecule warrant a thorough spectroscopic investigation. We have undertaken this spectroscopic study to identify and characterize the conformation(s) of AAMA using microwave spectroscopy. While conformational identification is commonly made by means of isotopic labeling, in this study, we have taken a different approach. The structure of AAMA contains three methyl groups, two of which cause torsion-rotation splittings in the microwave spectrum by virtue of having low  $V_3$  barriers. The analyses of these spectra have enabled determinations of two sets of angles that define the three dimensional orientations of the methyl groups'  $C_3$  axes in the principal inertial frame. These angles are shown to be unique to the  $C_7^{eq}$  conformational structure of AAMA and provide a structural identification without the need for isotopic labeling.

In general, the methyl torsional level structure when resolved can make isotopic substitution analyses difficult and subject to error. Rotational constants, for example, when used to obtain substitution coordinates require corrections for the effects of torsion-rotation interactions even for  $A$ -states fit to effective asymmetric rotor Hamiltonians. Herein, we describe methods implemented in a convenient software interface<sup>27</sup> for the “high-barrier” rotational analysis of the  $A$ - and  $E$ -torsional states for molecules possessing one or more methyl rotors.

## II. EXPERIMENT

During the course of this work, several samples of AAMA from different chemical manufacturers were used. For the initial survey scans of AAMA, the sample purity of a commercial sample (Chem-Impex International<sup>28</sup>) was  $>99\%$  and used without further purification. For a number of other experiments, a second commercial sample (BACHEM Biosciences, Inc.<sup>28</sup>) was also used at a stated purity  $>99\%$ . The  $^{15}\text{N}$  and  $^{13}\text{C}$  substituted compounds were custom synthesized as described below. To obtain sufficient vapor pressure prior to expansion, the nozzle reservoir was heated from 180 to 200 °C. Most amino acid and peptide related compounds can be somewhat unstable under elevated temperature con-

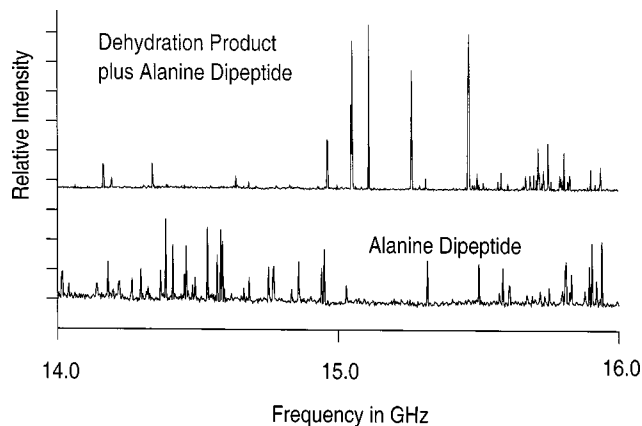


FIG. 2. FTMW spectrum observed using a brass reservoir nozzle where transitions from the dehydration product dominant. The lower spectrum observed using a glass coated reservoir consists almost entirely of transitions from AAMA.

ditions and AAMA appears to be no different. In a number of the experiments performed here, decomposition *via* dehydration occurred when the sample was heated. Furthermore, the custom synthesized isotopomers appeared to contain small amounts of two impurities which gave rise to additional lines in the spectrum. Their spectra were also assigned in this work and will be reported elsewhere. The thermal decomposition of AAMA was essentially eliminated by using a Silcosteel<sup>®</sup>-coating on the reservoir nozzle. Figure 2 shows the spectrum from 14 to 16 GHz that was obtained using an uncoated reservoir where the dehydration product dominates (top trace) and the coated reservoir (bottom trace) where only transitions from AAMA are present.

The rotational spectra were recorded using the Fourier-transform microwave (FTMW) spectrometers at NIST, which are described in detail elsewhere.<sup>29,30</sup> Survey scans were recorded by averaging the digitized free induction decays for 10–50 nozzle pulses followed by Fourier transformation at consecutive 500 kHz intervals. Uninterrupted scans covering 1 to 4 GHz intervals were sectioned together over the 12 to 20 GHz spectral region.

The molecular beam was produced by a 1.2 mm diam pulsed valve (General Valve series 9) oriented parallel to the microwave cavity axis. Heated samples of AAMA were expanded with a mixture of helium and neon (20%/80% by volume) at backing pressures of  $\approx 200$  kPa. The rotational temperature in the expansion under these conditions is typically  $\approx 2$  K.

Isotopically enriched forms of AAMA were prepared from the enriched precursor materials, <sup>15</sup>N-alanine and <sup>15</sup>N-methyl amine. The synthesis of AAMA isotopomers from alanine followed a route similar to that used to prepare isotopomers of alaninamide<sup>20</sup> and prolinamide.<sup>21</sup> The first reaction, of alanine with acetic anhydride, forms the acetyl group; this step also blocks the amine terminus from acting as a nucleophile in subsequent reactions. Next the carboxylic acid was esterified with *p*-nitrophenol and the coupling reagent dicyclohexylcarbodiimide. Finally, AAMA was formed by reacting the activated ester with anhydrous methyl amine generated in a vacuum line from methyl amine hydrochloride

and excess NaOH. Intermediate compounds were characterized by FTIR and FTNMR (300 MHz) spectroscopy. The final product was purified by repeated vacuum sublimations.

### III. THEORY

The molecular structure of AAMA contains three inequivalent methyl groups. For sufficiently low torsional barriers, the pure rotational spectrum will contain additional splittings from (i) the torsional level structure and (ii) torsional-overall rotational angular momentum coupling. The torsion-rotation Hamiltonians appropriate to such problems have been given before in both principal-axis and internal-axis frames for one top,<sup>31–33</sup> two equivalent tops,<sup>34–36</sup> two inequivalent tops<sup>37</sup> and *n*-tops<sup>38</sup> attached to an asymmetric molecule. For a single rotor, each torsional level,  $\nu$ , will split into an *A*- and doubly-degenerate *E*-state in the absence of torsion-rotation interactions. The number of split torsional states increases to five for two inequivalent rotors, i.e., *AA*-, *AE*-, *EA*-, and two *EE*-states and to 14 for three rotors: *AAA*-, *AAE*-, *AEA*-, *EAA*-, two *AEE*-, two *EAE*-, two *EEA*-, and four *EEE*-states. For *n*-methyl tops, torsion-rotation interactions will lift the  $2^k$ -fold degeneracy of the  $A_{n-k}E_k$ ,  $k \geq 1$  levels to give a total of  $3^n$  states for each rotational state pair,  $|J, |K|$ . Whereas kinetic coupling interactions between the tunneling rotors may be important for the  $A_{n-k}E_k$ ,  $k \geq 2$  levels, there will always be one  $A_{n-1}$ -state and  $n$   $A_{n-1}E$ -states where these interactions will be absent. For sufficiently high barriers, these states may be fit independently.<sup>34</sup> The analysis of the  $A_{n-1}E$ -state spectra can provide accurate structural data pertaining to principal axis orientation of the rotor(s) as well as the torsional barrier height(s). The close proximity of two or more methyl groups may require higher-order terms in the Fourier expansion of the torsional potential for an accurate description of the barriers.<sup>39</sup> Given the large geometrical separation of the methyl groups in AAMA (cf. Fig. 1), we shall assume the contributions of these higher-order terms are negligible.

The “high-barrier” Hamiltonian<sup>40,41</sup> has been used successfully to fit *A*- and *E*-state spectra obtained in both the microwave and UV for a wide variety of asymmetric-top molecules. AAMA has three nonequivalent methyl groups and therefore, lacks the elements of symmetry used to simplify the Hamiltonians given previously for two equivalent groups attached to asymmetric molecule.<sup>34–36</sup> For the general case of *n* rotors, the effective Hamiltonian for the  $A_n$  torsional level is

$$\hat{H}_A^{\text{eff}} = A_A \hat{P}_a^2 + B_A \hat{P}_b^2 + C_A \hat{P}_c^2 + \sum_{k=1}^n \sum_{g \neq g' = a, b, c} E_{00(k), gg'} \times (\hat{P}_g \hat{P}_{g'} + \hat{P}_{g'} \hat{P}_g) + (4\text{th-order terms}), \quad (1)$$

where the sum in  $k$  runs over  $n$  methyl rotors. Here,  $E_{00(k), ab} = F_{(k)} W_{00(k)}^{(2)} \rho_{a(k)} \rho_{b(k)}$ , etc. are the coefficients of cross terms that function to rotate the inertial frame and  $\rho_{g(k)} = \lambda_{g(k)} I_{\phi} / I_g$  ( $g = a, b, c$ ) are structural parameters defined in terms of the moments of inertia of the methyl group,  $I_{\phi(k)}$ , the whole molecule,  $I_g$ , and the direction cosines,  $\lambda_{g(k)}$ . These latter quantities specify the relative orientation of the threefold symmetry axis of the methyl rotor and prin-

principal inertial axes.  $W_{00(k)}^{(2)}$  ( $W_{\nu\sigma(k)}^{(2)}$ ) are the second-order perturbation coefficients calculated for the  $A$ -states ( $\sigma=0$ ) of the lowest torsional level ( $\nu=0$ ) and have been tabulated elsewhere.<sup>42</sup> The 4th-order terms have the same operator form as Watson's quartic centrifugal distortion parameters.<sup>43</sup> The coefficients of these terms may also include contributions from torsion-rotation interactions as described by Herschbach.<sup>41</sup> The  $A_n$ -state rotational constant,  $A_A$ , correct to second order in torsion-rotation interactions is

$$A_A = A_R + \sum_{k=1}^n F_{(k)} W_{00(k)}^{(2)} \rho_{a(k)}^2, \quad (2)$$

$$F_{(k)} = \frac{\hbar^2}{2I_{\phi(k)} r_{(k)}}, \quad (3)$$

$$r_{(k)} = 1 - \sum_{g=a,b,c} \lambda_{g(k)}^2 \frac{I_{\phi(k)}}{I_g}, \quad (4)$$

where  $F_{R(k)} = \hbar^2/2I_{\phi(k)}$  and  $A_R = \hbar^2/2I_a$ , etc., are the rigid-rotor constants of the  $k$ th methyl rotor and whole molecule, respectively. Similar expressions to Eq. (2) may be written for  $B_A$  and  $C_A$ .

The effective Hamiltonian for the  $A_{n-1}E$ -state includes additional terms that describe the angular momentum coupling of the internal rotor and the overall rotational motion of the molecule,

$$\begin{aligned} \hat{H}_{E(k)}^{\text{eff}} = & A_{E(k)} \hat{P}_a^2 + B_{E(k)} \hat{P}_b^2 + C_{E(k)} \hat{P}_c^2 + \sum_{g=a,b,c} D_{g(k)} \hat{P}_g \\ & + \sum_{g \neq g' = a,b,c} E_{0\pm 1(k),gg'} (\hat{P}_g \hat{P}_{g'} + \hat{P}_{g'} \hat{P}_g) \\ & + G_a \hat{P}_a^3 + (\text{4th-order terms}), \end{aligned} \quad (5)$$

where  $D_{g(k)} = F_{(k)} W_{0\pm 1(k)}^{(1)} \rho_{g(k)}$  and  $E_{0\pm 1(k),gg'} = F_{(k)} W_{0\pm 1(k)}^{(2)} \rho_{g(k)} \rho_{g'(k)}$ . We have explicitly truncated the power series to a single cubic term.  $W_{0\pm 1(k)}^{(1)}$  and  $W_{0\pm 1(k)}^{(2)}$  are the first- and second-order perturbation coefficients calculated for the  $E$ -torsional levels.<sup>42</sup> The rotational constants,  $A_{E(k)}$ , etc., now include the following second-order corrections:

$$A_{E(k)} = A_R + F_{(k)} W_{0\pm 1(k)}^{(2)} \rho_{a(k)}^2 + \sum_{k' \neq k} F_{(k')} W_{00(k')}^{(2)} \rho_{a(k')}^2. \quad (6)$$

The direction cosine,  $\lambda_{a(k)}$ , may be obtained from the parameters defined above and

$$\lambda_{a(k)} = \pm \frac{D_{a(k)} B_R C_R}{\sqrt{D_{a(k)}^2 B_R^2 C_R^2 + D_{b(k)}^2 A_R^2 C_R^2 + D_{c(k)}^2 A_R^2 B_R^2}}, \quad (7)$$

where we have used the property,  $\lambda_{a(k)}^2 + \lambda_{b(k)}^2 + \lambda_{c(k)}^2 = 1$ . Similar expressions for  $\lambda_{b(k)}$  and  $\lambda_{c(k)}$  are easily obtained by permutation of the parameters in the numerator of Eq. (7). Once the direction cosines have been determined, the coefficient,  $W_{0\pm 1(k)}^{(1)}$  may be calculated from the definition of  $D_{g(k)}$ . The reduced barrier parameter,  $s_{(k)}$ , is found from the tabulated values<sup>42</sup> of  $W_{0\pm 1(k)}^{(1)}$  and the corresponding values of  $W_{0\pm 1(k)}^{(2)}$  are used to obtain improved values of  $A_R$ ,  $B_R$ ,

$C_R$ , and  $\lambda_{g(k)}$ . The process must be iterated until self-consistent values of these parameters are obtained. Notice that the  $A_R$ , etc. include contributions from all rotors. Furthermore,  $F_{R(k)}$  may be calculated from Eqs. (2) and (6),

$$F_{R(k)} = \frac{(W_{00(k)}^{(2)} - W_{01(k)}^{(2)}) A_R^2 \lambda_{a(k)}^2}{r_{(k)} (A_A - A_{E(k)})}. \quad (8)$$

Analogous expressions may be written in terms of the  $B$  and  $C$  rotational constants. Finally, the torsional barrier is obtained from

$$V_{3(k)} = \frac{9}{4} s_{(k)} F_{(k)}. \quad (9)$$

A modified form of Eq. (5) has been found to give significantly improved fits of the  $A_{n-1}E$ -state spectra of AAMA, i.e.,

$$\begin{aligned} \hat{H}_{E(k)}^{\text{eff}} = & A'_{E(k)} \hat{P}_a^2 + B'_{E(k)} \hat{P}_b^2 + C'_{E(k)} \hat{P}_c^2 + D'_{a(k)} \hat{P}_a \\ & + \sum_{g \neq g' = a,b,c} E'_{gg'(k)} (\hat{P}_g \hat{P}_{g'} + \hat{P}_{g'} \hat{P}_g) + G'_{a(k)} \hat{P}_a^3 \\ & + (\text{4th-order terms}). \end{aligned} \quad (10)$$

Similar to the theoretical treatment of hindered rotation based on the internal axis method,<sup>44</sup> the Hamiltonian of Eq. (10) is transformed to a "rho" axis frame where  $\rho_{b(k)} = \rho_{c(k)} = 0$ . In effect, the Hamiltonian has been rotated eliminating the coefficients  $D_{b(k)}$  and  $D_{c(k)}$  of Eq. (5) from the fit.<sup>45</sup> The rotational transformation is most conveniently expressed in terms of the Euler angles,  $\phi$ ,  $\theta$ ,  $\chi$ , of the direction cosine matrix,<sup>46</sup>

$$\phi = \tan^{-1} \left( \frac{D_{c(k)}}{D_{b(k)}} \right), \quad (11)$$

$$\theta = \tan^{-1} \left( \frac{\sqrt{D_{b(k)}^2 + D_{c(k)}^2}}{D_{a(k)}} \right), \quad (12)$$

$$D'_{a(k)} = \pm \sqrt{D_{a(k)}^2 + D_{b(k)}^2 + D_{c(k)}^2}, \quad (13)$$

where  $\chi$  is arbitrary. The transformation introduces additional contributions to the coefficients of the cross terms,  $E'_{gg'}$ , already present in Eq. (5). In general, any two of the three cross terms,  $E'_{gg'}$ , are sufficient to affect this transformation. Consequently, the third cross term of Eq. (10) is highly correlated with the inertial parameters [as are all of the cross terms,  $E_{0\pm 1(k),gg'}$ , of Eq. (5)] and generally not varied in the fit. However, further improvements in the standard deviation of the fit are realized by fixing the third cross term at the optimal value obtained from refits of the data at stepped values of  $\chi$ . It is further noted that the transformation from Eq. (5) to Eq. (10) is *not* unitary (otherwise, identical results would be obtained). For example, the operator forms of the 4th order parameters are not subjected to this transformation. The matrix elements of these terms are calculated as in Eq. (5) but now in the  $\rho$ -axis frame.

The rotor axis angles and  $V_3$  barriers are obtained from the best-fit parameters of Eq. (10) after rotation via diagonalization of the inertial tensor back into the principal axis frame. The direction cosines for this transformation (i.e., the

eigenvectors) are used to redefine the components,  $D_{a(k)}$ ,  $D_{b(k)}$ , and  $D_{c(k)}$  from  $D'_{a(k)}$ . The rotor axis angles and  $V_3$  barriers are calculated as before with the aid of Eqs. (7) and (9). The graphical user interface (GUI) program, JB95,<sup>27</sup> provides an interface to all of the parameters in Eqs. (5) and (10) and the transformations between the principal axis and  $\rho$ -axis frames. A separate console-based program is also integrated with the GUI to perform the barrier calculations which include corrections up to 4th-order for one or more rotors.

## IV. RESULTS

### A. Dehydration product

Microwave spectra of AAMA were initially obtained using a brass reservoir nozzle heated to 180 °C. The top trace of Fig. 2 shows the observed spectrum from 14 to 16 GHz. Transitions were assigned to two separate spectra characteristic of *A*- and *E*-state methyl torsional state transitions. The rotational constants obtained from the least squares fit of the *A*-state spectrum are  $A = 2307.225(4)$  MHz,  $B = 1666.860(2)$  MHz, and  $C = 1041.390(2)$  MHz. These inertial parameters are, however, inconsistent with any possible conformational structure of AAMA. To verify this, rotational constants were calculated for different geometries defined by successive rotations about each of the two dihedral angles,  $\psi$  and  $\phi$ , at 1° intervals. These angles are defined in Fig. 1 for the  $C_7^{eq}$  structure. In general, the calculated constants were nearly always smaller than observed values. Additional spectra of the  $^{15}\text{N}$ - $^{14}\text{N}$ ,  $^{14}\text{N}$ - $^{15}\text{N}$ , and  $2$ - $^{13}\text{C}$  labeled isotopomers were also recorded using the brass nozzle assembly. The substitution coordinates determined from a Kraitchman analysis<sup>47</sup> identify a dehydration product formed by cyclization of the AAMA molecule followed by nucleophilic attack of the amide nitrogen lone pair at the carbonyl carbon of the acetyl. The analysis and structure of the dehydration product [3,5-dihydro-2,3,5-trimethyl-(9CI) 4H imidazole-4-one; CAS registry #32023-93-1] will be reported elsewhere.

### B. $A_n$ -state analyses of AAMA and AAMA( $^{15}\text{N}_2$ )

The upper trace in Fig. 3 shows the pure rotational spectrum of AAMA from 12 to 20 GHz obtained using the coated reservoir nozzle. Initial guesses for the *AA*-state rotational constants were obtained from the *ab initio* values reported for the  $C_7^{eq}$  structure.<sup>7</sup> Quantum numbers were first assigned to experimental frequencies for the strongest series of  $K_a = 0$  transitions and stepwise refinements in the fit to Eq. (1) were made by including increasingly higher  $K_a$  levels. AAMA contains two  $^{14}\text{N}$  nuclei and therefore, nuclear quadrupole coupling of the two  $I = 1$   $^{14}\text{N}$  nuclei results in a complex hyperfine splitting pattern for each rotational line. No attempt was made to fit the quadrupole structure but rather, the rotational line centers were estimated near the center of gravity of the clusters, which spanned up to  $\approx 1.0$  MHz in many cases. As a consequence of the broadened asymmetric lines, the observed minus calculated standard deviation of 52 assigned lines was 15 kHz, which is more than an order-of-magnitude larger than the measurement precision of 2 kHz. To eliminate the  $^{14}\text{N}$  hyperfine structure, the double  $^{15}\text{N}$

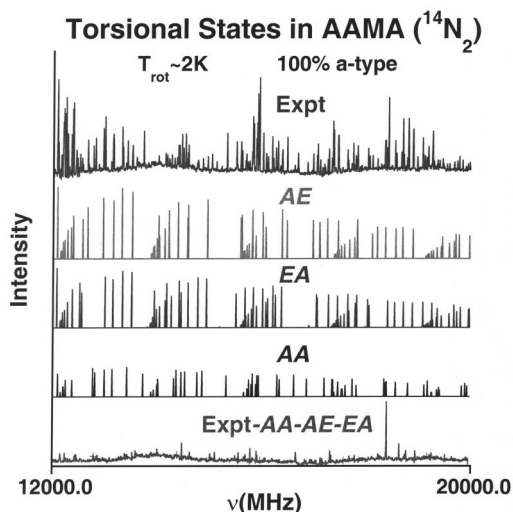


FIG. 3. Observed spectrum of AAMA (top) and simulated spectra of the *AA*-, *AE*-, and *EA*-states. The observed lines remaining following the removal of transitions from the three simulated spectra are shown as the bottom trace.

structure of AAMA was synthesized and its spectrum analyzed in a similar manner. The assignment of 60 transitions resulted in an O–C standard deviation of 1.5 kHz. The best-fit rotational constants for both isotopomers that include Watson's quartic distortion parameters in the *A*-reduction (representation  $I'$ ) are given in Table VII. The standard uncertainties ( $k = 1$  or  $1\sigma$ ) reported are those obtained directly from the fit. Despite the difference in the accuracy of the measurements, the distortion parameters of AAMA and AAMA( $^{15}\text{N}_2$ ) are nearly the same to within the experimental uncertainty.

### C. *AE*-state and *EA*-state analyses of AAMA and AAMA( $^{15}\text{N}$ )

The rotational analysis of the *AE*-states of AAMA began with the removal of the *AA*-state transitions using features of the software.<sup>27</sup> Beginning with the *AA*-state rotational constants, the  $K_a = 0$  lines were first included in the least-squares fit. Adding in  $K_a = 1$  transitions required variation of the linear term,  $D_a$ , in Eq. (5) and upon including the  $K_a = 2$  lines, all three linear parameters could be reliably fit. With the observed-calculated residuals near 100 kHz, it became increasingly difficult to predict the locations of the higher  $K_a$  lines using the Hamiltonian of Eq. (5). Adding the 4th-order terms of Eq. (5) to the fit resulted in uncertainties in the parameters that exceeded their values and were, therefore, meaningless. To proceed further with the assignment, it was necessary to transform to the Hamiltonian given in Eq. (10) using Eqs. (11)–(13). Refits of the data that included 4th-order terms reduced the O–C standard deviation to  $\approx 16$  kHz. The predictive quality of the model permitted the assignment of all remaining lines.

Similar fitting strategies were used to assign a second *EA*-state of AAMA and the *AE*- and *EA*-states of AAMA( $^{15}\text{N}_2$ ). The magnitudes of the tunneling splittings in the *AE*- and *EA*-states relative to the corresponding transi-

TABLE I. Observed transition frequencies for the AA-state of AAMA(<sup>14</sup>N<sub>2</sub>).

$J'$	$K'_a$	$K'_c$	$J''$	$K''_a$	$K''_c$	Transition frequency (MHz)	Obs-Calc (kHz)
7	1	7	6	1	6	10 550.7732	-3.5
7	0	7	6	0	6	10 567.7615	-1.4
8	1	8	7	1	7	11 987.9980	-2.8
8	0	8	7	0	7	11 994.8827	-1.5
7	3	5	6	3	4	12 093.8768	19.3
7	5	3	6	5	2	12 200.6303	-16.2
7	5	2	6	5	1	12 208.0505	-12.2
7	4	4	6	4	3	12 243.4977	0.3
7	2	5	6	2	4	12 770.1904	9.5
7	3	4	6	3	3	12 813.5615	-19.2
8	2	7	7	2	6	12 991.0964	-4.7
8	1	7	7	1	6	13 138.5161	10.0
9	1	9	8	1	8	13 422.5412	-7.4
9	0	9	8	0	8	13 425.2326	5.9
8	3	6	7	3	5	13 730.9939	8.1
8	6	3	7	6	2	13 927.5314	2.8
8	4	5	7	4	4	14 011.1655	-17.3
9	2	8	8	2	7	14 455.3290	6.2
9	1	8	8	1	7	14 529.4237	15.9
8	3	5	7	3	4	14 763.5786	4.8
10	1	10	9	1	9	14 855.9791	0.4
10	0	10	9	0	9	14 856.9908	0.6
9	3	7	8	3	6	15 316.4725	-2.4
9	6	4	8	6	3	15 716.8430	13.6
9	6	3	8	6	2	15 721.9192	-1.7
9	4	6	8	4	5	15 751.8020	13.9
9	5	5	8	5	4	15 793.7805	16.9
9	2	7	8	2	6	15 822.5754	-4.8
9	5	4	8	5	3	15 878.4562	0.5
10	2	9	9	2	8	15 903.3624	9.6
10	1	9	9	1	8	15 937.5303	5.5
11	1	11	10	1	10	16 288.9771	3.9
11	0	11	10	0	10	16 289.3542	7.4
9	4	5	8	4	4	16 338.5182	0.4
9	3	6	8	3	5	16 612.4535	2.1
10	3	8	9	3	7	16 853.1874	-26.6
10	2	8	9	2	7	17 194.5719	-30.8
11	2	10	10	2	9	17 342.5423	-51.9
11	1	10	10	1	9	17 357.4700	9.7
10	5	6	9	5	5	17 594.2119	1.2
10	3	7	9	3	6	18 324.8632	40.2
11	3	9	10	3	8	18 349.7460	25.2
10	4	6	9	4	5	18 377.3983	3.3
11	2	9	10	2	8	18 547.9920	-0.7
12	2	11	11	2	10	18 777.5796	-15.6
12	1	11	11	1	10	18 783.8080	13.2
11	4	8	10	4	7	19 096.3956	2.4
11	5	7	10	5	6	19 378.9128	1.5
11	5	6	10	5	5	19 815.6154	-13.9
11	3	8	10	3	7	19 881.5665	-33.3
12	2	10	11	2	9	19 920.2540	20.7

tions in the AA-state are shown in Fig. 4. The experimental lines for all assigned states are listed in Tables I–VI. The parameters obtained in the principal axis frames from least squares fits to Eq. (5) are summarized in Table VII for both AE-states and both isotopomers. In all four cases, the observed–calculated (O–C) standard deviations are more than 100-fold larger than the measurement precision. The parameters obtained in the  $\rho$ -axis frame using Eq. (10) are given in Table VIII. For both AE-states of the <sup>14</sup>N<sub>2</sub> iso-

TABLE II. Observed transition frequencies for the AE-state of AAMA(<sup>14</sup>N<sub>2</sub>).

$J'$	$K'_a$	$K'_c$	$J''$	$K''_a$	$K''_c$	Transition frequency (MHz)	Obs-Calc (kHz)
7	0	7	6	0	6	10 453.2092	-3.0
6	4	2	5	4	1	10 468.5861	-16.3
6	4	3	5	4	2	10 508.4023	7.8
6	3	3	5	3	2	10 619.8316	-23.4
6	3	4	5	3	3	10 640.0639	-1.0
7	1	7	6	1	6	10 652.7318	-9.2
8	1	8	7	1	7	12 083.6737	-2.5
7	5	2	6	5	1	12 189.9702	13.3
7	5	3	6	5	2	12 219.8373	14.2
7	4	3	6	4	2	12 280.5500	7.5
7	4	4	6	4	3	12 345.1538	-36.1
7	3	5	6	3	4	12 387.4287	8.8
7	3	4	6	3	3	12 569.9446	-5.2
7	2	5	6	2	4	12 665.2999	0.1
8	1	7	7	1	6	12 962.9949	2.5
8	2	7	7	2	6	13 156.3794	3.6
9	0	9	8	0	8	13 316.4866	0.7
9	1	9	8	1	8	13 515.0294	-1.4
8	6	2	7	6	1	13 915.4338	12.8
8	6	3	7	6	2	13 940.2677	-13.0
8	3	6	7	3	5	14 016.5659	-28.0
8	4	5	7	4	4	14 214.2720	13.1
8	2	6	7	2	5	14 217.0338	-34.8
9	1	8	8	1	7	14 382.4658	14.8
8	3	5	7	3	4	14 565.3728	31.9
9	2	8	8	2	7	14 584.8991	26.4
10	0	10	9	0	9	14 748.3857	3.8
10	1	10	9	1	9	14 946.5999	-20.5
9	3	7	8	3	6	15 586.4175	36.0
9	2	7	8	2	6	15 609.8217	5.2
9	6	3	8	6	2	15 701.7415	-3.1
9	5	4	8	5	3	15 805.2453	-11.5
10	1	9	9	1	8	15 809.0383	-19.9
9	5	5	8	5	4	15 875.3448	2.5
10	2	9	9	2	8	16 011.2685	-1.6
9	4	6	8	4	5	16 064.7587	8.0
9	4	5	8	4	4	16 066.7157	-10.3
11	0	11	10	0	10	16 180.3543	15.2
11	1	11	10	1	10	16 378.3442	9.1
9	3	6	8	3	5	16 467.5005	-10.6
10	2	8	9	2	7	16 960.4375	5.6
10	3	8	9	3	7	17 092.8104	-8.8
11	1	10	10	1	9	17 238.2533	15.8
11	2	10	10	2	9	17 439.1750	-2.5
12	0	12	11	0	11	17 612.3330	5.5
10	4	7	9	4	6	17 805.4030	26.5
12	1	12	11	1	11	17 810.1003	-15.8
10	4	6	9	4	5	18 089.2640	-3.8
10	3	7	9	3	6	18 184.8284	15.7
11	2	9	10	2	8	18 343.4882	9.2
11	3	9	10	3	8	18 536.9841	-7.1
12	1	11	11	1	10	18 668.5192	7.3
12	2	11	11	2	10	18 868.4232	9.5
13	0	13	12	0	12	19 044.3214	-8.6
13	1	13	12	1	12	19 241.9305	0.1
11	4	8	10	4	7	19 429.0378	-33.3
11	5	6	10	5	5	19 568.4282	2.6
11	5	7	10	5	6	19 659.7797	4.4
12	2	10	11	2	9	19 752.9807	-34.2
12	3	10	11	3	9	19 958.8340	16.2

TABLE III. Observed transition frequencies for the EA-state of AAMA(<sup>14</sup>N<sub>2</sub>).

<i>J'</i>	<i>K'<sub>a</sub></i>	<i>K'<sub>c</sub></i>	<i>J''</i>	<i>K''<sub>a</sub></i>	<i>K''<sub>c</sub></i>	Transition frequency (MHz)	Obs-Calc (kHz)
8	1	8	7	1	7	12 074.4413	-17.0
7	5	2	6	5	1	12 182.8025	12.6
7	5	3	6	5	2	12 221.5505	6.1
7	4	3	6	4	2	12 279.1598	-29.1
7	4	4	6	4	3	12 372.9663	21.8
7	3	5	6	3	4	12 375.2710	19.3
7	2	5	6	2	4	12 511.5306	3.4
7	3	4	6	3	3	12 552.4602	-7.6
8	1	7	7	1	6	12 999.0339	-18.5
8	2	7	7	2	6	13 144.3970	20.9
9	0	9	8	0	8	13 335.2913	14.0
9	1	9	8	1	8	13 505.9161	-4.5
8	4	4	7	4	3	14 139.4231	2.7
8	2	6	7	2	5	14 175.0871	-1.0
8	4	5	7	4	4	14 262.0441	-9.0
9	1	8	8	1	7	14 407.4111	2.9
9	2	8	8	2	7	14 578.4929	7.3
10	0	10	9	0	9	14 767.5122	-3.5
9	3	7	8	3	6	15 500.0640	-11.2
9	2	7	8	2	6	15 673.1400	13.6
9	6	3	8	6	2	15 689.9349	13.1
9	5	4	8	5	3	15 797.4250	4.6
10	1	9	9	1	8	15 830.0929	-16.2
9	5	5	8	5	4	15 892.4151	15.7
10	2	9	9	2	8	16 004.0732	-11.6
9	4	5	8	4	4	16 066.8954	-11.4
9	4	6	8	4	5	16 098.5828	-31.0
11	0	11	10	0	10	16 199.8835	0.4
9	3	6	8	3	5	16 252.9498	-3.8
11	1	11	10	1	10	16 369.9302	3.3
10	3	8	9	3	7	17 046.9118	29.6
11	1	10	10	1	9	17 257.9349	4.9
11	2	10	10	2	9	17 430.9250	6.4
10	7	4	9	7	3	17 447.5480	-16.5
12	0	12	11	0	11	17 632.3290	9.5
10	4	7	9	4	6	17 771.5222	-18.6
12	1	12	11	1	11	17 802.1687	-7.7
10	3	7	9	3	6	18 005.8364	5.4
10	4	6	9	4	5	18 036.3500	-2.2
11	2	9	10	2	8	18 389.7929	5.7
11	3	9	10	3	8	18 524.5545	-25.6
12	1	11	11	1	10	18 687.7477	3.8
12	2	11	11	2	10	18 859.6342	11.4
13	0	13	12	0	12	19 064.7824	-9.5
13	1	13	12	1	12	19 234.5029	3.7
11	4	8	10	4	7	19 334.4617	2.3
11	5	7	10	5	6	19 712.9749	18.5
12	2	10	11	2	9	19 782.8049	-5.1
12	3	10	11	3	9	19 954.1211	0.1

TABLE IV. Observed transition frequencies for the AA-state of AAMA(<sup>15</sup>N<sub>2</sub>).

<i>J'</i>	<i>K'<sub>a</sub></i>	<i>K'<sub>c</sub></i>	<i>J''</i>	<i>K''<sub>a</sub></i>	<i>K''<sub>c</sub></i>	Transition frequency (MHz)	Obs-Calc (kHz)
5	2	3	4	2	2	9151.2533	3.6
6	1	5	5	1	4	10 287.7900	-0.1
6	3	4	5	3	3	10 348.2820	-0.4
6	4	3	5	4	2	10 404.9771	3.9
6	4	2	5	4	1	10 447.0492	-1.0
7	1	7	6	1	6	10 485.3792	0.2
7	0	7	6	0	6	10 502.1037	1.5
6	3	3	5	3	2	10 762.4760	1.3
4	3	2	3	2	1	10 917.9131	-1.4
6	2	4	5	2	3	10 977.4912	-0.8
4	3	1	3	2	1	10 985.2998	0.2
5	2	3	4	1	3	11 313.5061	-0.6
7	2	6	6	2	5	11 431.0332	-0.1
7	1	6	6	1	5	11 686.0871	-0.1
8	1	8	7	1	7	11 913.5842	0.0
8	0	8	7	0	7	11 920.3459	-0.6
7	5	3	6	5	2	12 130.1740	1.2
7	4	4	6	4	3	12 172.7188	0.5
7	4	3	6	4	2	12 301.6052	0.4
7	2	5	6	2	4	12 695.2605	-2.7
7	3	4	6	3	3	12 741.8365	-1.7
4	4	0	3	3	0	12 798.9048	-1.5
4	4	1	3	3	1	12 807.6118	-1.5
4	4	0	3	3	1	12 808.8696	-0.9
8	2	7	7	2	6	12 911.8674	-3.4
8	1	7	7	1	6	13 057.2851	-0.1
5	3	3	4	2	3	13 113.3846	0.4
9	1	9	8	1	8	13 339.1477	-1.3
9	0	9	8	0	8	13 341.7747	0.2
6	2	4	5	1	4	13 492.2469	-1.1
8	3	6	7	3	5	13 649.5083	-2.2
8	5	4	7	5	3	13 911.8498	0.1
8	4	5	7	4	4	13 929.9747	-2.2
8	5	3	7	5	2	13 940.2752	-0.9
8	4	4	7	4	3	14 237.0675	0.1
8	2	6	7	2	5	14 277.9648	1.2
9	2	8	8	2	7	14 366.7410	-0.1
9	1	8	8	1	7	14 439.6405	1.1
5	4	1	4	3	1	14 488.9341	0.9
5	4	2	4	3	2	14 545.2562	1.8
8	3	5	7	3	4	14 679.9981	1.1
10	1	10	9	1	9	14 763.6151	0.0
10	0	10	9	0	9	14 764.6051	0.4
6	3	4	5	2	4	15 108.9326	2.3
9	3	7	8	3	6	15 224.8021	4.6
9	6	4	8	6	3	15 626.2263	-0.4
9	6	3	8	6	2	15 631.3767	-0.7
9	4	6	8	4	5	15 660.0114	-1.1
9	5	5	8	5	4	15 702.8472	-0.1
9	2	7	8	2	6	15 725.8960	1.7
9	5	4	8	5	3	15 788.1846	-0.3
10	2	9	9	2	8	15 805.5794	-1.9
10	1	9	9	1	8	15 839.1259	-0.8
11	1	11	10	1	10	16 187.6570	1.4
11	0	11	10	0	10	16 188.0202	-0.1
9	4	5	8	4	4	16 247.8542	-2.1
9	3	6	8	3	5	16 516.7340	1.1
10	3	8	9	3	7	16 751.5264	-1.3
10	2	8	9	2	7	17 088.5022	0.0
10	3	7	9	3	6	18 216.9175	2.5

pomer, the O-C standard deviations of more than 50 assigned lines improve by more than 10-fold and like the AA-state, are limited in accuracy to ≈15 kHz from the unresolved hyperfine structure. Even more remarkable are the improvements realized for the AE- and EA-states of the <sup>15</sup>N<sub>2</sub> isotopomer. The O-C standard deviations of the fits are both <3 kHz and nearly 100-fold better than obtained in the principal axis frames using Eq. (5).

The improved fits using Eq. (10) are primarily a result of the ability to adequately model in 4th order the centrifugal

TABLE V. Observed transition frequencies for the *AE*-state of AAMA(<sup>15</sup>N<sub>2</sub>).

<i>J'</i>	<i>K'<sub>a</sub></i>	<i>K'<sub>c</sub></i>	<i>J''</i>	<i>K''<sub>a</sub></i>	<i>K''<sub>c</sub></i>	Transition frequency (MHz)	Obs–Calc (kHz)
6	1	6	5	1	5	9164.4464	1.6
6	1	5	5	1	4	10 121.0933	0.9
7	0	7	6	0	6	10 389.1549	1.0
6	4	3	5	4	2	10 447.8969	–0.7
6	3	3	5	3	2	10 560.1288	1.2
6	3	4	5	3	3	10 578.1053	4.0
7	1	7	6	1	6	10 586.0096	0.8
4	3	2	3	2	2	10 724.0660	–0.4
6	2	4	5	2	3	10 865.7746	0.3
4	3	1	3	2	1	11 420.6105	8.1
7	1	6	6	1	5	11 492.1676	–0.6
7	2	6	6	2	5	11 633.8855	0.5
8	0	8	7	0	7	11 811.7172	0.0
8	1	8	7	1	7	12 008.0234	0.5
7	5	3	6	5	2	12 149.2989	1.3
7	4	4	6	4	3	12 274.4685	–1.1
7	3	5	6	3	4	12 312.9820	–2.1
4	4	1	3	3	1	12 415.0542	2.5
7	3	4	6	3	3	12 500.7375	–0.7
7	2	5	6	2	4	12 591.8291	–1.8
8	1	7	7	1	6	12 884.1858	–1.9
8	2	7	7	2	6	13 074.8319	0.4
9	0	9	8	0	8	13 234.5522	–0.1
9	1	9	8	1	8	13 430.4483	–2.1
8	6	2	7	6	1	13 834.9903	–2.2
8	6	3	7	6	2	13 859.7070	0.4
8	5	3	7	5	2	13 904.7189	–2.5
8	3	6	7	3	5	13 930.4572	–0.7
8	5	4	7	5	3	13 950.9724	–1.0
5	4	2	4	3	2	14 123.0482	–3.1
9	1	8	8	1	7	14 294.8066	–0.2
8	3	5	7	3	4	14 484.9634	–0.2
9	2	8	8	2	7	14 494.4686	1.1
6	3	3	5	2	3	14 632.3517	–6.9
10	0	10	9	0	9	14 657.5095	1.5
10	1	10	9	1	9	14 853.1090	–0.6
9	3	7	8	3	6	15 490.3527	0.3
9	2	7	8	2	6	15 515.7129	0.0
9	7	2	8	7	1	15 552.3554	2.0
9	6	3	8	6	2	15 611.2550	0.4
9	6	4	8	6	3	15 647.2165	1.5
10	1	9	9	1	8	15 712.5303	–1.2
9	5	4	8	5	3	15 714.8487	–1.1
9	5	5	8	5	4	15 784.5502	0.8
10	2	9	9	2	8	15 912.0108	0.1
9	4	6	8	4	5	15 971.1317	1.2
9	4	5	8	4	4	15 977.5126	–0.4
11	0	11	10	0	10	16 080.5242	0.3
11	1	11	10	1	10	16 275.8913	–1.0
9	3	6	8	3	5	16 374.1627	1.1
11	1	10	10	1	9	17 132.8048	0.8
11	2	10	10	2	9	17 331.0429	0.5
11	2	9	10	2	8	18 231.8758	0.3

distortion and torsion-rotation interactions. The importance of these higher order terms are also realized from refits of the *AA*-states. For example, the O–C standard deviations increase to 119 and 75 kHz for AAMA and AAMA(<sup>15</sup>N<sub>2</sub>), respectively, when the 4th-order parameters are excluded from the fits.

TABLE VI. Observed transition frequencies for the *EA*-state of AAMA(<sup>15</sup>N<sub>2</sub>).

<i>J'</i>	<i>K'<sub>a</sub></i>	<i>K'<sub>c</sub></i>	<i>J''</i>	<i>K''<sub>a</sub></i>	<i>K''<sub>c</sub></i>	Transition frequency (MHz)	Obs–Calc (kHz)
6	3	3	5	3	2	10 566.9569	–0.8
7	1	7	6	1	6	10 578.1463	0.7
6	3	4	5	3	3	10 619.7537	0.2
6	2	4	5	2	3	10 711.8042	–0.9
7	1	6	6	1	5	11 544.7515	7.0
7	2	6	6	2	5	11 599.0990	4.1
8	0	8	7	0	7	11 828.7020	5.5
8	1	8	7	1	7	11 999.9594	0.6
7	5	3	6	5	2	12 151.3809	0.7
7	4	3	6	4	2	12 208.4316	–1.2
7	4	4	6	4	3	12 302.6540	–0.6
7	3	5	6	3	4	12 305.5876	–2.3
7	2	5	6	2	4	12 440.8451	5.7
7	3	4	6	3	3	12 479.7767	–3.1
8	1	7	7	2	6	12 917.5002	0.4
8	2	7	7	2	6	13 064.8397	1.7
9	0	9	8	0	8	13 251.7397	–2.7
9	1	9	8	1	8	13 422.4834	–2.5
8	6	3	7	6	2	13 856.9531	–0.6
8	3	6	7	3	5	13 864.2402	–1.2
8	5	3	7	5	2	13 896.6444	0.5
8	5	4	7	5	3	13 957.8591	–2.1
9	1	8	8	1	7	14 317.7567	2.9
9	2	8	8	2	7	14 489.2993	0.5
10	0	10	9	0	9	14 675.0274	0.4
10	1	10	9	1	9	14 845.4313	1.3
9	3	7	8	3	6	15 411.9885	–0.9
9	7	2	8	7	1	15 539.7754	0.3
9	7	3	8	7	2	15 568.2479	0.0
9	2	7	8	2	6	15 574.9725	–5.8
9	6	3	8	6	2	15 599.5389	–1.2
9	6	4	8	6	3	15 645.8689	–1.2
9	5	4	8	5	3	15 706.7203	3.4
10	1	9	9	1	8	15 731.8237	1.4
9	5	5	8	5	4	15 802.2454	5.6
10	2	9	9	2	8	15 905.9308	–4.0
9	4	5	8	4	4	15 974.7431	0.1
9	4	6	8	4	5	16 007.9618	–0.9
11	0	11	10	0	10	16 098.4381	0.3
9	3	6	8	3	5	16 161.5454	–2.3
11	1	11	10	1	10	16 268.6037	0.9
11	1	10	10	1	9	17 150.8204	1.9

#### D. Remaining lines

Simulated spectra of the *AA*-, *AE*-, and *EA*-states of the <sup>14</sup>N<sub>2</sub> isotopomer are shown in Fig. 3 together with the observed spectrum of AAMA. The remaining transitions following the removal of all lines predicted for these states are shown as the lowest trace in Fig. 3. Attempts to assign the remaining weak lines were not successful. They are not likely associated with the third rotor's *AE*-state since transitions are expected to appear with intensity comparable to the assigned spectra. Therefore, we attribute the remaining lines to the two *EE*-states which are expected to be twofold weaker from nuclear spin weight arguments alone.<sup>37</sup>

#### V. DISCUSSION

As discussed above, the presence of three methyl rotors in the structure of AAMA gives rise to a total of 14 torsional

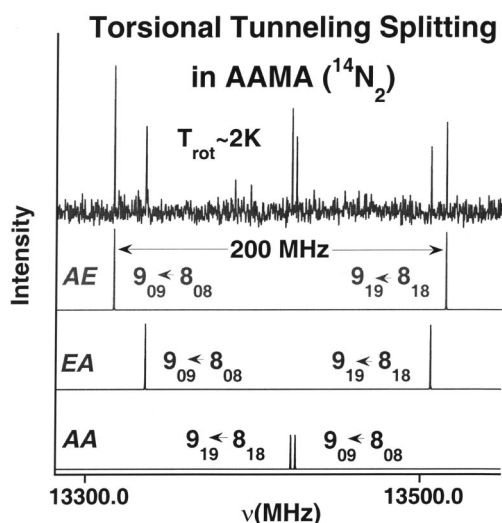


FIG. 4. Expanded region of the AAMA ( $^{14}\text{N}$ ) spectrum illustrating the magnitude of the tunneling splitting from torsion-rotation interactions for the *AE*- and *EA*-states compared to the asymmetry splitting of the *AA*-state doublet,  $9_{09} \leftarrow 8_{08}$ ,  $9_{19} \leftarrow 8_{18}$ .

states. Furthermore, predictions from *ab initio* theory indicate the  $C_5$  conformer is from 143 to 614  $\text{cm}^{-1}$  higher in energy than the  $C_7^{\text{eq}}$  structure<sup>7</sup> and therefore, likely to be populated in the 413 K reservoir nozzle prior to expansion. If the conformer population is “frozen in” during the expansion, the intensity of the transitions arising from the  $C_5$  conformer are predicted between 10% and 40% of that observed for corresponding transitions of the  $C_7^{\text{eq}}$  conformer, assuming dipole moments of comparable magnitude for both structures. When taken together, the FTMW spectrum of AAMA at 2 K might be expected to contain up to  $2 \times 14$  independent subspectra.

The analyses of these spectra, however, have revealed that three states account for the vast majority of the features

in the spectrum. Of these states, the *AA*-state is fit to a standard *A*-reduction Hamiltonian and two *AE*-states are fit to effective torsion-rotation Hamiltonians. These same three states have been assigned for the AAMA( $^{15}\text{N}_2$ ) isotopomer at 10-fold higher precision. In the following sections, the results derived from the torsion-rotation parameters are used to identify from among the 28 possible states (i) the methyl rotor associated with each *AE*-state and (ii) the conformational structure of AAMA. We conclude by comparing the experimental structural data with predictions from *ab initio* theory.

### A. Methyl torsional state analyses of AAMA and AAMA( $^{15}\text{N}_2$ )

The parameters and uncertainties determined for the *AA*-state (Table VII), *AE*-, and *EA*-states in the  $\rho$ -axis frames (Table VIII) were simultaneously included in a program to iteratively refine the perturbation coefficients, rotor axis angles and  $V_3$  barriers according to the procedures described above. These calculations were first performed using the lower uncertainty parameters of the AAMA( $^{15}\text{N}_2$ ) isotopomer in order to obtain  $F_{R(k)}$  values for each rotor using Eq. (8). The *A*, *B*, and *C* rotational constants were used for the  $F_{R(k)}$  determinations weighted in proportion to the differences in the *AA*- and *AE*-state (and *EA*-state) rotational constants. Since  $F_{R(k)}$  is expected to be isotope independent, a similar calculation was performed for AAMA but for fixed values of  $F_{R(k)}$ . A summary of the results and uncertainties for both isotopomers is given in Table IX. The standard uncertainties are dominated by the uncertainty in  $F_{R(k)}$  as obtained from propagation of the uncertainties in the parameters.

As evident in Table IX, the rotor axis angles and  $V_3$  barriers are well-determined for both *AE*-states and both isotopomers. The calculated barriers are nearly independent of isotopomer as expected: the *AE*-state barriers for AAMA and

TABLE VII. Rotational constants of AAMA and AAMA( $^{15}\text{N}_2$ ) obtained from fits in the principal axis frames. Type A standard uncertainties (i.e.,  $k=1$  or  $1\sigma$ ) are given, as determined from the least-squares fit.

Parameter	AAMA( $^{14}\text{N}_2$ )			AAMA( $^{15}\text{N}_2$ )		
	<i>AA</i>	<i>AE</i>	<i>EA</i>	<i>AA</i>	<i>AE</i>	<i>EA</i>
<i>A</i> /MHz	1717.37(1)	1712.25(5)	1713.0(1)	1706.2163(3)	1701.19(2)	1702.1(2)
<i>B</i> /MHz	992.922(1)	992.867(4)	991.37(1)	987.3589(1)	987.309(3)	958.87(1)
<i>C</i> /MHz	716.492(1)	716.062(3)	716.357(7)	712.011 05(9)	711.595(2)	711.879(9)
$\Delta_J$ /kHz	0.142(5)			0.1390(6)		
$\Delta_{JK}$ /kHz	-0.30(2)			-0.340(3)		
$\Delta_K$ /kHz	1.8(5)			0.84(2)		
$\delta_J$ /kHz	0.031(3)			0.0351(3)		
$\delta_K$ /kHz	0.21(5)			0.121(4)		
$D_a$ /MHz		356.7(1)	418.5(7)		352.5(1)	416.9(5)
$D_b$ /MHz		32.9(5)	237.6(2)		34.1(4)	233.1(2)
$D_c$ /MHz		98.69(3)	84.49(7)		97.49(3)	84.72(8)
$G_a$ /MHz			0.08(5)		-0.023(7)	0.32(5)
$\kappa$	-0.447	-0.448	-0.448	-0.446	-0.443	-0.447
$\Delta I/\mu\text{Å}^2$ <sup>a</sup>	-97.90	-99.31	-99.31	-98.26	-98.74	-97.62
Assigned	52	60	49	60	53	42
$\sigma$ /kHz <sup>b</sup>	15.2	195	395	1.5	146	345

<sup>a</sup>Inertial defect,  $\Delta I \equiv 505\,379(1/C - 1/A - 1/B)$ .

<sup>b</sup>Observed - calculated standard deviation of the fit.

AAMA( $^{15}\text{N}_2$ ) are 98.4(2) and 98.65(8)  $\text{cm}^{-1}$ ; the *EA*-state barriers are 84.0(3) and 84.1(1)  $\text{cm}^{-1}$ , respectively. In contrast, some change in the rotor axis angles might be anticipated for the two isotopomers since the orientation of the principal axis frame will generally have a mass dependence. The differences in these angles are, in fact, small with magnitudes not exceeding  $1^\circ$ .

The observed differences in the *AA*- and *AE*-state (and *EA*-state) “rigid-rotor” constants determined using Eqs. (2) and (6) are also reported in Table IX. These differences provide some measure of the validity of the approximations made in the high-barrier model. The predicted values of  $\Delta A_R$ ,  $\Delta B_R$ , and  $\Delta C_R$  for the *AE*-states of both isotopomers are nearly within the experimental uncertainty of the fitted constants. This is, however, not the case for *EA*-states where, for example, the values of  $\Delta B_R$  are near 0.1 MHz. Systematic differences are seen to exist for all of the parameters although of smaller magnitude. In an attempt to account for these differences, additional barrier calculations were performed that included denominator and 4th-order corrections to the rotational constants.<sup>41</sup> The corrections amount to  $<0.001$  MHz and do not explain these differences. Refits of the data that included the cubic terms,  $G_b P_b^3$ ,  $G_c P_c^3$  and cross terms,  $G_{abb}(P_b^2 P_a + P_b P_a P_b + P_a P_b^2)$ , etc., as well as the parameter,  $L_a P_a^5$ , did not improve this situation. Although the reasons are not yet fully understood, the discrepancies are small and do not invalidate the use of this model.

## B. Conformational assignment of AAMA and AAMA( $^{15}\text{N}_2$ )

The rotor axis angles determined for the *AE*- and *EA*-states have provided structural information pertinent to the conformational form of AAMA. The orientation of the amide and carbonyl methyl groups are seen to depend principally on the torsional angles,  $\phi$  and  $\psi$ , that define the backbone conformation as a result of the rigid framework of the two

TABLE VIII. Rotational constants of AAMA and AAMA( $^{15}\text{N}_2$ ) from fits in  $\rho$ -axis frames. Type A standard uncertainties (i.e.,  $k=1$  or  $1\sigma$ ) are given, as determined from the least-squares fit.

Parameter	AAMA( $^{14}\text{N}_2$ )		AAMA( $^{15}\text{N}_2$ )	
	<i>AE</i>	<i>EA</i>	<i>AE</i>	<i>EA</i>
$A'/\text{MHz}$	1636.07(2)	1512.97(2)	1625.094(2)	1508.076(4)
$B'/\text{MHz}$	893.98(11)	1143.85(1)	888.11(1)	1130.668(3)
$C'/\text{MHz}$	891.25(13)	763.916(5)	886.92(2)	760.844(1)
$\Delta_J/\text{kHz}$	0.186(7)	0.49(5)	0.173(1)	0.53(1)
$\Delta_{JK}/\text{kHz}$	-1.63(10)	-1.9(3)	-0.97(2)	-2.27(9)
$\Delta_K/\text{kHz}$	4.2(3)	0.2(2)	1.61(8)	0.60(5)
$\delta_J/\text{kHz}$		0.27(3)	0.091(3)	0.298(9)
$\delta_K/\text{kHz}$	1.1(1)	-0.52(7)	0.73(2)	-0.44(2)
$D'_a/\text{MHz}$	371.78(1)	489.86(1)	367.372(1)	487.738(2)
$E'_{bc}/\text{MHz}$	+107.61(2)	-109.997(5)	+107.842(2)	-110.815(1)
$E'_{ab}/\text{MHz}$	-115.48(5)	+335.133(8)	-112.031(6)	-330.406(2)
$E'_{ac}/\text{MHz}$	-235.1558 <sup>a</sup>	-15.095 59 <sup>a</sup>	+235.1558 <sup>b</sup>	-15.095 59 <sup>b</sup>
$G'_a/\text{MHz}$	-0.0274(4)	-0.0278(3)	-0.026 47(9)	-0.028 31(7)
Assigned	60	49	53	42
$\sigma/\text{kHz}^c$	16.3	15.6	1.96	2.62

<sup>a</sup>Fixed at corresponding  $^{15}\text{N}$  value.

<sup>b</sup>Optimal values obtained by scanning  $\chi$  and fixed in fit.

<sup>c</sup>Observed–calculated standard deviation of the fit.

peptide chains. The following error function is defined to correlate the experimentally derived angles with the specific methyl groups and to identify the conformational form of AAMA,

$$E(\varphi, \psi) = \sqrt{\sum_{k=1}^2 \sum_{g=a,b,c} [(\theta_{g(k)}^{\text{expt}} - \theta_{g(k)}^{\text{calc}})]^2}. \quad (14)$$

The direction cosine angles,  $\theta_{a(k)}^{\text{calc}}$ , etc., are the rotor axis angles for each rotor,  $k$ , calculated in the principal axis frame as a function of the two Ramachandran angles,  $\phi$  and  $\psi$  (see Fig. 1). All other structural parameters were fixed at the values calculated for the B3LYP/6-31G\* optimized  $C_{7\text{eq}}^7$  geom-

TABLE IX. Experimentally derived angles of the methyl-rotor axes relative to the *a*, *b*, and *c* principal axes and methyl torsional parameters and barriers of both AAMA and AAMA( $^{15}\text{N}_2$ ).

	AAMA( $^{14}\text{N}_2$ )		AAMA( $^{14}\text{N}_2$ )		AAMA( $^{15}\text{N}_2$ )		AAMA( $^{15}\text{N}_2$ )	
	<i>AA</i>	<i>AE</i>	<i>AA</i>	<i>EA</i>	<i>AA</i>	<i>AE</i>	<i>AA</i>	<i>EA</i>
$\theta_a/^\circ$	...	34.41(12)	...	47.68(2)	...	34.44(1)	...	47.208(4)
$\theta_b/^\circ$	...	82.58(10)	...	48.42(1)	...	82.20(1)	...	49.001(3)
$\theta_c/^\circ$	...	56.62(12)	...	70.97(2)	...	56.69(1)	...	70.788(4)
$W^{(1)}$	...	-0.249 994	...	-0.360 226	...	-0.248 782	...	-0.359 459
$s$	...	8.179 192	...	6.777 151	...	8.199 950	...	6.785 104
$W^{(2)}$	0.269 729	-0.132 472	0.367406	-0.175 958	0.268494	-0.131 895	0.366767	-0.175 692
$F_R/\text{cm}^{-1}$		5.300 <sup>a</sup>		5.467 <sup>a</sup>		5.300(4) <sup>b</sup>		5.467(7) <sup>b</sup>
$V_3/\text{cm}^{-1}$		98.4(2)		84.0(3)		98.65(8)		84.1(1)
$\Delta A_R/\text{MHz}^c$		-0.076		-0.064		-0.002 <sup>b</sup>		-0.080 <sup>b</sup>
$\Delta B_R/\text{MHz}^c$		-0.002		+0.096		-0.003		+0.093
$\Delta C_R/\text{MHz}^c$		+0.021		-0.066		+0.018		-0.061
$A_R/\text{MHz}^d$				1710.97(8)				1699.85(8)
$B_R/\text{MHz}^d$				991.89(9)				986.36(9)
$C_R/\text{MHz}^d$				716.12(6)				711.64(6)

<sup>a</sup>Fixed at the  $F_R$  values determined for the  $^{15}\text{N}_2$  isotopomers.

<sup>b</sup>Average  $F_R$  value determined using Eq. (8) and weighted in proportion to  $A_A - A_{E(k)}$ ,  $B_A - B_{E(k)}$ , and  $C_A - C_{E(k)}$ .

<sup>c</sup> $\Delta A_R = A_R^A - A_R^E$ , etc.

<sup>d</sup>Average of *AA*-, *AE*-, and *EA*-state values.

etry. A further restriction,  $0^\circ \leq \theta_{g(k)}^{calc} \leq 90^\circ$ , is imposed since the signs of the experimental angles are not determined [see Eq. (7)]. Furthermore, six permutations are possible for the two sets of observed angles and three methyl groups and therefore, six surfaces were examined. Of these possibilities, the two surfaces that have the deepest global minima are shown in Fig. 5. In the top panel, the rotor axis angles of the acetyl ( $T_1$ ) and amide ( $T_2$ ) methyl groups are correlated with those derived for the *AE*- and *EA*-states, respectively, while these associations are reversed in the lower panel. The top surface is, in fact, the only one of the six that has  $E(\phi, \psi) < 10^\circ$  and serves to uniquely associate the two methyl rotors and  $V_3$  barriers with the experimental data. The global minimum value of  $2.5^\circ$  is located at  $\phi = -80.1^\circ$  and  $\psi = 71.3^\circ$  and unambiguously identifies the conformational form of AAMA as the  $C_7^{eq}$  structure. Therefore, we find the methyl top attached to the acetyl end of AAMA has a barrier of  $98.4(2) \text{ cm}^{-1}$  and the rotor attached to the amide group has a barrier of  $84.0(3) \text{ cm}^{-1}$ . The absence of lines in the spectra from the  $C_5$  conformer suggests efficient collisional relaxation of this conformer to the  $C_7^{eq}$  form during the jet-cooled expansion.

### C. Comparisons with *ab initio* theory

AAMA has served as a model system for conformational studies of proteins and peptides and because of its small size, has been examined in depth at various levels of theory. The backbone conformation in the  $C_7^{eq}$  form is strongly influenced by the directional character and strength of the amide-to-carbonyl intramolecular hydrogen bond which, in turn, effects the principal axis orientations of the amide and carbonyl methyl groups. Furthermore, the torsional barrier heights and rotational constants of the two methyl rotors are sensitive to the local steric and electronic environments at the termini of the hydrogen bond.

For two points of comparison with these results, *ab initio* studies were performed on the  $C_7^{eq}$  structure of AAMA( $^{14}\text{N}_2$ ) at B3LYP/6-31G\* and MP2/6-31G\* levels of theory using the GAUSSIAN program suite.<sup>48</sup> At the optimized geometries, the rotational constants, the rotor axis angles and rotor constants,  $F_R$ , were determined for each of the three methyl groups. Additional optimizations were performed to estimate the  $V_3$  torsional barrier heights. For these calculations, each methyl group was rotated about its  $C_3$  axis by  $60^\circ$  and held fixed while all other coordinates were permitted to fully relax. The *ab initio* results are summarized in Tables X and XI.

The B3LYP and MP2/6-31G\* calculated rotational constants are within 1.4% and 0.7%, respectively, of the experimental "rigid-rotor" constants for the  $^{14}\text{N}_2$  isotopomer. The rotor axis angles predicted for the acetyl methyl ( $T_1$ ) and methyl amide ( $T_2$ ) groups are only in modest agreement with the experimental data, with deviations greater than  $2^\circ$  in some cases. The average deviations of these angles improve by  $<20\%$  at the global minimum values of  $\phi$  and  $\psi$  given by Eq. (14) (see Table X). The  $V_3$  barriers are overestimated at the B3LYP level of theory for both the acetyl and amide methyl groups by 14% and 4%, respectively while this trend is reversed at the MP2 level. Interestingly, the MP2 theory

dramatically underestimates the torsional barrier of the acetyl methyl by more than  $60 \text{ cm}^{-1}$ . Both levels of theory predict the  $V_3$  barrier of the side chain methyl group ( $T_3$ ) at  $>900 \text{ cm}^{-1}$  which explains why a third *AE*-state is not resolved; for  $V_3$  barriers  $>700 \text{ cm}^{-1}$ , the *A/E*-state splittings would be smaller than the 2 kHz measurement precision. Finally, notice that the calculated  $F_R$  constants of the acetyl methyl group are in excellent agreement with experiment but are

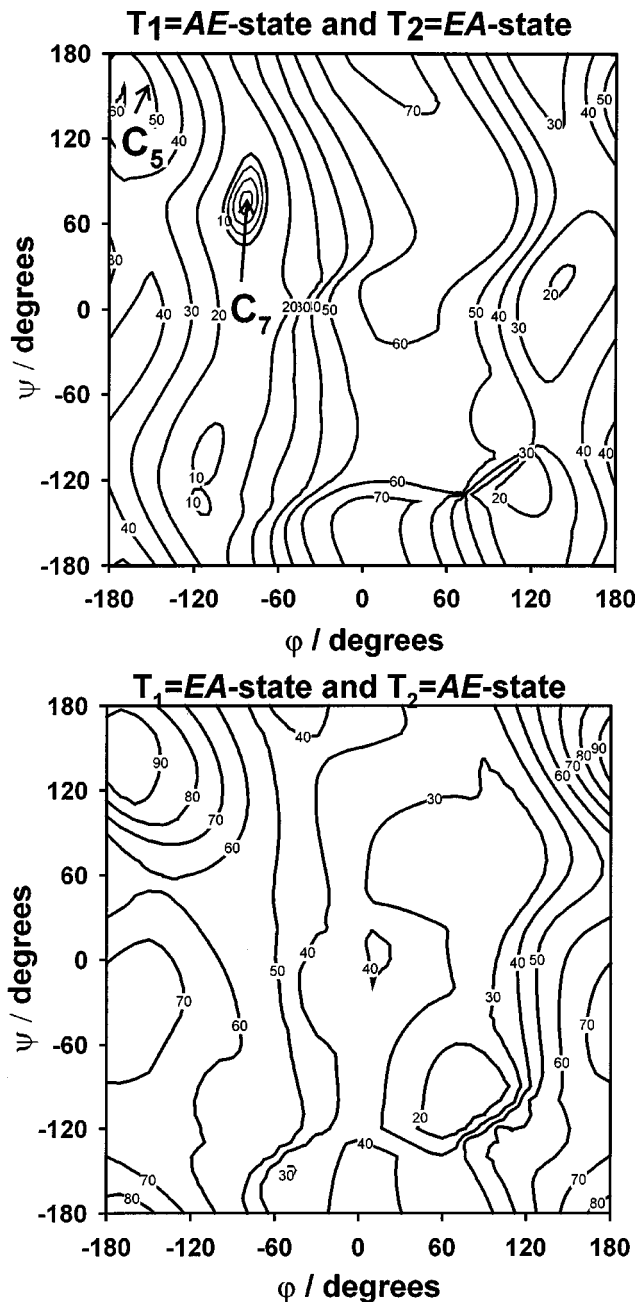


FIG. 5. Contour plots of the error surfaces defined by Eq. (14) for the  $T_1$  and  $T_2$  methyl rotors as a function of the two Ramachandran angles,  $\phi$  and  $\psi$  (cf. Fig. 1). For each pair of angles, the principal axis frame is found via diagonalization of the inertial tensor matrix. The rotor axis angles are calculated from the principal axis coordinates. All structural parameters except  $\phi$  and  $\psi$  are held fixed at the optimized values obtained from the B3LYP/G-31G\* optimized  $C_7^{eq}$  structure. The regions corresponding to the two lowest energy structures,  $C_7^{eq}$  and  $C_5$ , are indicated. Contours inside  $10^\circ$  for the  $C_7^{eq}$  structure are shown at  $2^\circ$  steps.

TABLE X. Observed and calculated rotational constants and dihedral angles for the  $C_7^{eq}$  structure of AAMA at the B3LPY/6-31G\* and MP2/6-31G\* levels of theory.

	$C_7^{eq}$		$C_7^{eq}$		$C_5$
	B3LYP <sup>a</sup>	O–C	MP2 <sup>a</sup>	O–C	MP2 <sup>a</sup>
$A/\text{MHz}$	1691.9	+19.1	1699.6	+11.4	2869.0
$B/\text{MHz}$	983.5	+8.4	992.7	–8.1	657.9
$C/\text{MHz}$	706.1	–10.0	719.9	–3.8	595.5
$\phi/^\circ$ <sup>b</sup>	–82.8	+2.7	–83.1	+3.1	158.4
$\psi/^\circ$ <sup>b</sup>	+72.7	–1.4	+77.8	+5.2	–161.3
$E(\phi, \psi)/^\circ$ <sup>c</sup>	3.2	–0.7	4.3	–0.8	32
$\Delta E/\text{kJ mol}^{-1}$ <sup>d</sup>	0		0		7.35

<sup>a</sup>Same as theoretical results reported in Ref. 7.

<sup>b</sup> $\phi(C_3N_1C_1C_2)$  and  $\psi(N_2C_2C_1N_1)$  define dihedral angles. Observed values defined at the global minimum of Eq. (14).

<sup>c</sup>Defined according to Eq. (14).

<sup>d</sup> $C_5$  energy given relative to  $C_7^{eq}$ . RHF  $\Delta E = 1.71 \text{ kJ mol}^{-1}$  from Ref. 7.

underestimated by 3%–4% for the amide methyl group at both levels of theory.

## VI. SUMMARY AND CONCLUSIONS

This report details the first spectroscopic evidence for amide hydrogen-to-carbonyl oxygen hydrogen bonds between peptide residues in the structures of small biomolecules, and it illustrates the utility of gas-phase spectroscopy in identifying and characterizing the large-scale structural motifs of biomolecules. Similar hydrogen bonding networks between peptide groups stabilizes the protein  $\alpha$ -helix and  $\beta$ -sheet tertiary structures. This conformation requires at least two peptide bonds, while the amide-to-amine intramolecular hydrogen bond is favored if only one peptide bond is present. The ability to identify dipeptide conformations suggests that it soon may be possible to explore the structures of larger polypeptides using Fourier-transform microwave spectroscopy coupled with high-level theory.

Rotational spectra have been recorded for the  $^{14}\text{N}_2$  and  $^{15}\text{N}_2$  isotopomers of AAMA, and three torsional states ( $AA$ ,  $AE$ , and  $EA$ ) have been assigned in each spectrum. The rotor axis angles derived from the torsion-rotation parameters of the  $AE$ - and  $EA$ -states identify the acetyl methyl and methyl amide groups with barriers of 98.4(2) and 84.0(3)  $\text{cm}^{-1}$ , respectively, and the conformation of AAMA as  $C_7^{eq}$ . This structure is characterized by a seven membered ring and an intramolecular hydrogen bond from the amide nitrogen to the

carbonyl oxygen. These data are unbiased by the interactions of a solvent environment and therefore, may serve as benchmark data for tests of theoretical models and more importantly, for validation of current force fields derived for peptides and proteins.

The barriers to internal rotation of the methyl amide and acetyl methyl groups are consistent with the  $V_3$  barriers determined for other biomimetic molecules.  $A$ - and  $E$ -state spectra have recently been assigned for a number of acetamide derivatives with methyl groups in both the acetyl position and the  $N$ -methyl positions. Several other molecules with the same basic framework of alanine dipeptide have also been examined. A future goal of this work is to compare theoretical algorithms developed to assign rotational spectra of molecules containing one or more symmetric rotors. To this end, four independent theoretical methods have been used to analyze various molecules in this data set. In this paper, the JB95 program<sup>27</sup> has been used. For other molecules in this series, Kleiner,<sup>33</sup> Ohashi,<sup>49</sup> and Hirota<sup>37</sup> have employed their fitting programs.

## ACKNOWLEDGMENTS

M. J. Tubergen wishes to acknowledge the financial support for this research from the U.S. National Science Foundation (CHE-9700833). The authors would like to thank Jon T. Hougen at NIST and Professor Paul Sampson at Kent State University for helpful discussions.

- C. L. Brooks III, M. Karplus, and B. M. Pettitt, "Proteins: A Theoretical Perspective of Dynamics, Structure, and Thermodynamics," *Advances in Chemical Physics* (Wiley, New York, 1988), Vol. LXXI, p. 259, and references therein.
- T. Head-Gordon, M. Head-Gordon, M. J. Frisch, C. L. Brooks III, and J. A. Pople, *J. Am. Chem. Soc.* **113**, 5989 (1991), and references therein.
- H.-J. Böhm and S. Brode, *J. Am. Chem. Soc.* **113**, 7129 (1991).
- C. L. Brooks III and D. A. Case, *Chem. Rev.* **93**, 2487 (1993), and references therein.
- I. R. Gould, W. D. Cornell, and I. H. Hillier, *J. Am. Chem. Soc.* **116**, 9250 (1994).
- L. Schäfer, I. S. Bin Dress, R. F. Frey, C. Van Alsenoy, and J. D. Ewbank, *THEOCHEM* **338**, 71 (1995).
- K. J. Jalkanen and S. Suhai, *Chem. Phys.* **208**, 81 (1996).
- C. H. Yu, M. A. Norman, L. Schäfer, M. Ramek, A. Peeters, and C. van Alsenoy, *J. Mol. Struct.* **567**, 361 (2001).
- W.-G. Han, K. J. Jalkanen, M. Elstner, and S. Suhai, *J. Phys. Chem. B* **102**, 2587 (1998).
- C.-D. Poon, E. T. Samulski, C. F. Weise, and J. C. Weisshaar, *J. Am. Chem. Soc.* **122**, 5642 (2000).
- G. T. Fraser, L.-H. Xu, R. D. Suenram, and C. L. Lugez, *J. Chem. Phys.* **112**, 6209 (2000).

TABLE XI. Calculated methyl rotor axis angles in the principal axis frame,  $V_3$  barrier heights, and rotor rotational constants for the  $C_7^{eq}$  structure of AAMA at the B3LPY/6-31G\* and MP2/6-31G\* levels of theory.

	Acetyl ( $T_1$ )				Amide ( $T_2$ )				Side chain ( $T_3$ )	
	B3LYP	O–C	MP2	O–C	B3LYP	O–C	MP2	O–C	B3LYP	MP2
$\theta_a/^\circ$	33.85	+0.56	33.94	+0.47	48.69	–1.01	49.21	–1.53	78.15	78.19
$\theta_b/^\circ$	85.28	–2.70	85.39	–2.81	47.17	+1.25	48.70	–0.28	12.21	12.07
$\theta_c/^\circ$	56.57	+0.05	56.46	+0.16	71.36	–0.39	68.23	+2.74	87.04	87.56
$V_3/\text{cm}^{-1}$	111.9	–13.5	30.7	+67.7	87.17	–3.17	70.1	+13.9	921	1141
$F_R/\text{cm}^{-1}$	5.310	–0.010	5.306	–0.006	5.275	+0.192	5.288	+0.179	5.304	5.301

- <sup>12</sup>G. T. Fraser, R. D. Suenram, and C. L. Lugez, *J. Phys. Chem.* **104**, 1141 (2000).
- <sup>13</sup>G. T. Fraser, R. D. Suenram, and C. L. Lugez, *J. Phys. Chem. A* **105**, 9859 (2001).
- <sup>14</sup>R. D. Brown, P. D. Godfrey, J. W. V. Storey, and M.-P. Bassez, *J. Chem. Soc. Chem. Commun.* **13**, 547 (1978).
- <sup>15</sup>R. D. Suenram and F. J. Lovas, *J. Mol. Spectrosc.* **72**, 372 (1978).
- <sup>16</sup>R. D. Suenram and F. J. Lovas, *J. Am. Chem. Soc.* **102**, 7180 (1980).
- <sup>17</sup>P. D. Godfrey and R. D. Brown, *J. Am. Chem. Soc.* **117**, 2019 (1995).
- <sup>18</sup>F. J. Lovas, Y. Kawashima, J.-U. Grabow, R. D. Suenram, G. T. Fraser, and E. Hirota, *Astrophys. J. Lett.* **455**, L201 (1995).
- <sup>19</sup>P. D. Godfrey, S. Firth, L. D. Hatherley, R. D. Brown, and A. P. Pierlot, *J. Am. Chem. Soc.* **115**, 9687 (1993).
- <sup>20</sup>R. J. Lavrich, J. O. Farrar, and M. J. Tubergen, *J. Phys. Chem. A* **103**, 4659 (1999).
- <sup>21</sup>K. A. Kuhls, C. A. Centrone, and M. J. Tubergen, *J. Am. Chem. Soc.* **120**, 10194 (1998).
- <sup>22</sup>R. J. Lavrich, C. R. Torok, and M. J. Tubergen, *J. Phys. Chem. A* **106**, 8013 (2002).
- <sup>23</sup>R. J. Lavrich, R. D. Suenram, and M. J. Tubergen (unpublished results).
- <sup>24</sup>R. J. Lavrich and M. J. Tubergen, *J. Am. Chem. Soc.* **122**, 2938 (2000).
- <sup>25</sup>F. L. Bettens, R. P. A. Bettens, R. D. Brown, and P. D. Godfrey, *J. Am. Chem. Soc.* **122**, 5856 (2000).
- <sup>26</sup>(a) R. B. Corey, *J. Am. Chem. Soc.* **60**, 1598 (1938); (b) R. Degeilh and R. E. Marsh, *Acta Crystallogr.* **12**, 1007 (1959); (c) F. L. Hirshfeld, *Acta Crystallogr., Sect. A: Cryst. Phys., Diffr., Theor. Gen. Crystallogr.* **A32**, 239 (1976); (d) D. L. Dorset, *ibid.* **47**, 510 (1991).
- <sup>27</sup>(a) W. A. Majewski, J. F. Pfanstiel, D. F. Plusquellic, and D. W. Pratt, *Laser Techniques in Chemistry*, edited by A. B. Myers and T. R. Rizzo (Wiley, New York, 1995), Vol. XXIII, pp. 101–148; (b) D. F. Plusquellic, R. D. Suenram, B. Maté, J. O. Jensen, and A. C. Samuels, *J. Chem. Phys.* **115**, 3057 (2001).
- <sup>28</sup>In order to adequately describe certain aspects of the experimental procedures it is necessary to use specific names. The use of these names does not imply an endorsement by NIST in any way.
- <sup>29</sup>R. D. Suenram, F. J. Lovas, W. Pereyra, G. T. Fraser, and A. R. Hight Walker, *J. Mol. Spectrosc.* **181**, 67 (1997).
- <sup>30</sup>R. D. Suenram, J.-U. Grabow, A. Zuban, and I. Leonov, *Rev. Sci. Instrum.* **70**, 2127 (1999).
- <sup>31</sup>R. C. Woods, *J. Mol. Spectrosc.* **21**, 4 (1966).
- <sup>32</sup>X.-Q. Tan, W. A. Wajewski, D. F. Plusquellic, and D. W. Pratt, *J. Chem. Phys.* **94**, 7721 (1991).
- <sup>33</sup>I. Kleiner, J. T. Hougen, J.-U. Grabow, S. P. Belov, M. Yu. Tretyakov, and J. Cosleou, *J. Mol. Spectrosc.* **179**, 41 (1996).
- <sup>34</sup>J. D. Swalen and C. C. Constain, *J. Chem. Phys.* **31**, 1562 (1959).
- <sup>35</sup>P. U. De Haag, R. Spooren, M. Ebben, L. Meerts, and J. T. Hougen, *Mol. Phys.* **69**, 265 (1990).
- <sup>36</sup>X.-Q. Tan, D. J. Clouthier, R. H. Judge, D. F. Plusquellic, J. L. Tomer, and D. W. Pratt, *J. Chem. Phys.* **95**, 7862 (1991).
- <sup>37</sup>Y. Kawashima, R. D. Suenram, and E. Hirota (unpublished).
- <sup>38</sup>R. C. Woods, *J. Mol. Spectrosc.* **22**, 49 (1967).
- <sup>39</sup>K. M. Gough, B. R. Henry, and T. A. Wildman, *J. Mol. Struct.* **124**, 71 (1985).
- <sup>40</sup>E. Wilson, Jr., C. C. Lin, and D. R. Lide, Jr., *J. Chem. Phys.* **23**, 136 (1953).
- <sup>41</sup>D. R. Herschbach, *J. Chem. Phys.* **31**, 91 (1959).
- <sup>42</sup>D. R. Herschbach, *J. Chem. Phys.* **27**, 975 (1957).
- <sup>43</sup>D. Kivelson and E. B. Wilson, Jr., *J. Chem. Phys.* **20**, 1575 (1952); S. R. Polo, *Can. J. Phys.* **35**, 880 (1957).
- <sup>44</sup>K. T. Hecht and D. M. Dennison, *J. Chem. Phys.* **26**, 31 (1957).
- <sup>45</sup>A. Held, B. B. Champagne, and D. W. Pratt, *J. Chem. Phys.* **95**, 8732 (1991).
- <sup>46</sup>R. N. Zare, *Angular Momentum: Understanding Spatial Aspects in Chemistry and Physics* (Wiley, New York, 1988).
- <sup>47</sup>W. Gordy and R. L. Cook, *Microwave Molecular Spectra*, 3rd ed. (Wiley-Interscience, New York, 1984).
- <sup>48</sup>M. J. Frisch, G. W. Trucks, H. B. Schlegel *et al.*, GAUSSIAN 98, Revision A.7, Gaussian, Inc., Pittsburgh, PA, 1998.
- <sup>49</sup>N. Ohashi, Y. Kawashima, R. D. Suenram, and J. T. Hougen (unpublished).